STRESS ANALYSIS AND STATIC TEST OF A THREE CELL BEAM

BY

LT. RICHARD L. HALL, USN.

Thesis (M.S.) University of Michigan.

JUNE 1952

STRESS ANALYSIS AND STATIC TEST OF A THREE CELL BEAM

INTRODUCTION

An aircraft wing consists of structural members capable of resisting bending, torsional and shear loads. Insofar as the stress analysis of the wing is concerned, the structural members resisting each of these loads can be considered separately. In the consideration of bending loads, wing structures may be typed according to the bending-load resistant material. For example, all bending material may be concentrated in the spar caps or distributed around the periphery of the profile. The analysis of the first type treats the wing covering as ineffective in bending. This is a reasonable conclusion, inasmuch as the sheet-metal covering will buckle at a very low load and the load carrying ability insofar as bending is concerned, is therefore negligible. As for the second type, the distributed bending material consists of spanwise stiffening members. These members are in the form of stringers, corrugations, and inner skins fastened to the covering metal. However, on the compression side of the wing the metal sheet covering will buckle at relatively low loads which necessitates the use of effective widths. Hence, the stress analysis of such a structure considers the skin as partially effective in bending.

At present there is the necessity of constructing aircraft wings with comparatively thick metal sheet covering. This increase of covering thickness permits the wing to carry relatively high airloads before buckling of the skin on the compression side, thus the skin is fully effective in bending. The stress analysis of this type of wing is the subject of this report.

PART I

ANALYSIS

THREE CELL BEAM WITH SKIN FULLY EFFECIVE IN BENDING

PART I

ANALYSIS

THREE CELL BEAM WITH SKIN FULLY EFFECTIVE IN BENDING

The object of this analysis is to develop the shear flow equations for a three cell beam with skin fully effective in bending. The resulting equations will apply for a beam loaded with shear, bending and torsional loads.

Consider a three cell beam with a general profile (e.g., any airfoil shape) as shown in Figure 1.

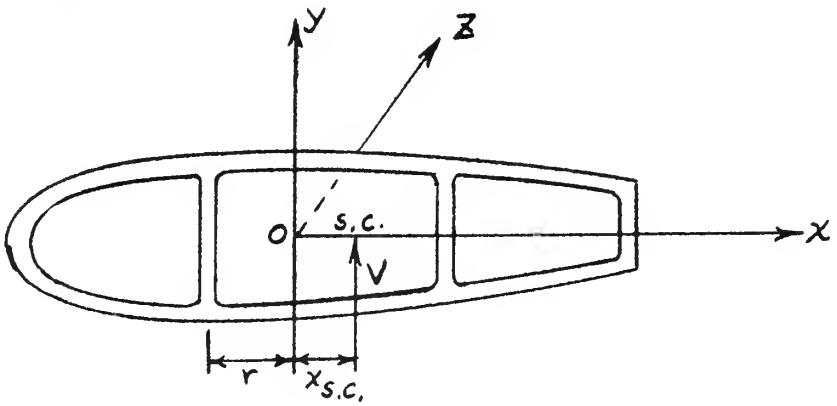

Figure 1

Refering to Figure 1.

O = centroid of cross section.

$x_{s.c.}$ = distance from centroid to shear center.

V = shear force in y direction (through shear center).

Initial Assumptions:

1. Principal axes are y and x axes, where x axis is chord line.
2. Wing planform contains no taper.
3. Load applied through shear center in y direction.

The shear flow designations are as shown in Figure 2.

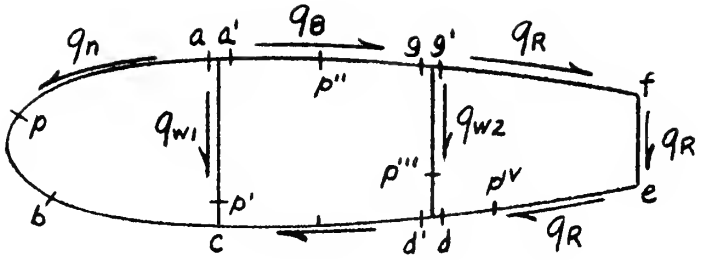

Figure 2

Referring to Figure 2.

q_n = Shear flow at any point nose skin.

q_B = Shear flow at any point on upper skin of center cell.

q_R = Shear flow at any point on rear cell skin.

q_C = Shear flow at any point on bottom skin of center cell.

q_{w1} = Shear flow at any point on front web.

q_{w2} = Shear flow at any point on second web.

q_a = Value of q_n at point a.

$q_{a'}$ = Value of q_b at point a'.

q_d = Value of q_R at point d.

Consider now the span wise forces acting on section p a of Figure 2, as shown in Figure 3. From equilibrium of spanwise forces:

$$P + \frac{dP}{dZ} - P + q_n dZ - q_a dZ = 0$$

$$q_a - q_n = \left|\frac{dP}{dZ}\right|_{ap}$$

where subscript ap indicates region from point a to point b.

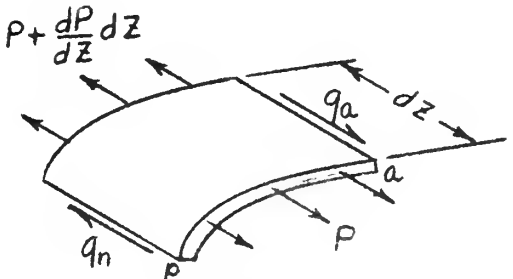

Figure 3

$$f_b = \frac{-M_x y}{I_x}$$

where f_b = Stress due to bending.

y = Distance from x axis.

I_x = Moment of inertia about x axis.

M_x = Bending moment about x axis.

Thus: $$P = \int_{ap} \frac{M_{xy}}{I_x} dA = -\frac{M_x}{I_x} \int_{ap} ydA = \frac{-M_x}{I_x} Q^x_{ap}$$

where Q^x_{ap} = moment of area from a to p about x axis.

But $$\frac{dM}{dZ} = V \text{ (i.e., shear force)}$$

Hence: $$\frac{dP}{dZ} = \frac{VQ^x_{ap}}{I_x} - M_x \frac{d}{dZ}\left(\frac{Q^x_{ap}}{I_x}\right)$$

Note: The second term in right side of above equation equals zero for non-tapered wing.

Therefore:

$$q_n = q_a + \frac{VQ^x_{ap}}{I_x} \qquad (1)$$

Points a and a' as shown in Figure 2 are points adjacent to either side of web-skin junction. Figure 4 shows the spanwise forces acting on section aa'p'.

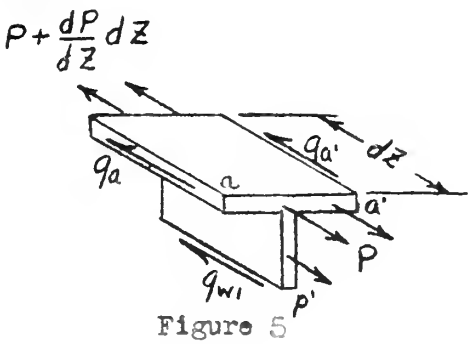

Figure 5

From Figure 5:

$$q_a + q_{a'} + q_{w1} = -\frac{dP}{dZ} = \frac{VQ^x_{ap'}}{I_x}$$

$$q_{w1} = -q_a - q_{a'} + \frac{VQ^x_{ap'}}{I_x} \qquad (2)$$

Considering spanwise forces acting on section a'p'' (Fig. 2 and), the equilibrium equation gives:

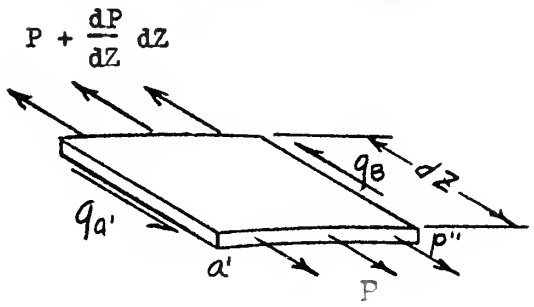

$$q_{a'} - q_B = \left(\frac{dP}{dZ}\right)_{a'p''} = -\frac{VQ^x_{a'p''}}{I_x}$$

or

$$q_B = q_{a'} + \frac{VQ^x_{a'p''}}{I_x} \qquad (3)$$

Figure 5

Considering spanwise forces acting upon section p" g' (Fig. 2 and 5), the equilibrium equation gives:

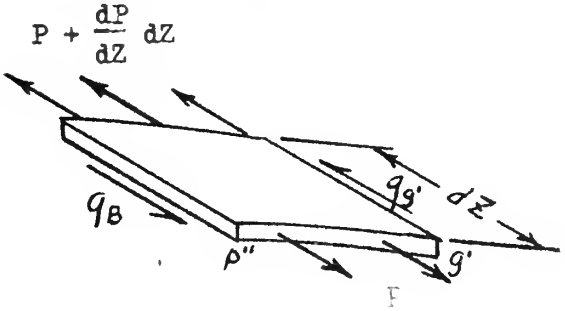

$$-q_{g'} + q_B = \left(\frac{dP}{dZ}\right)_{p''g'} = -\frac{VQ^x_{p''g'}}{I_x}$$

from which

$$q_{g'} = q_B + \frac{VQ^x_{p''g'}}{I_x}$$

Figure 6

and from equation 3, $q_{g'} = q_{a'} + \frac{VQ^x_{a'p''}}{I_x} + \frac{VQ^x_{p''g}}{I_x} = q_{a'} + \frac{VQ^x_{ag}}{I_x}$ (B)

Considering spanwise forces acting upon section gp"' (Fig. 2 and 6), the equilibrium equation gives:

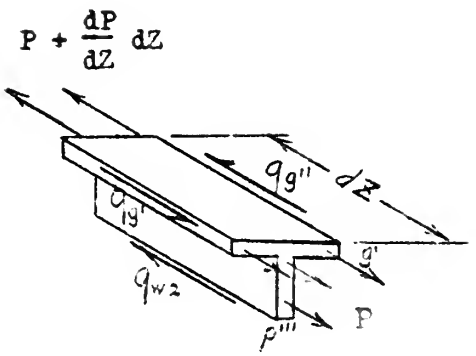

$$q_{w2} + q_{g''} - q_{g'} = -\left(\frac{dP}{dZ}\right)_{gp'''} = \frac{VQ^{x}_{gp'''}}{I_x}$$

or from equation B,

$$q_{w2} = -q_{g''} + q_{g'} + \frac{VQ^{x}_{ag}}{I_x} + \frac{VQ^{x}_{gp'''}}{I_x} \quad (C)$$

Figure 7

Considering spanwise forces acting upon section g''p'^{V} (Fig. 2 and 8), the equilibrium equation gives:

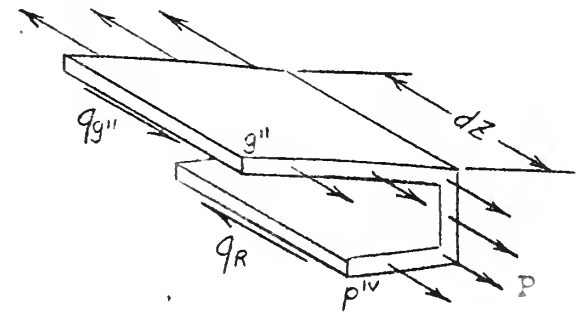

$$q_R - q_{g''} = -\left(\frac{dP}{dZ}\right)_{gp'^{V}} = \frac{VQ^{x}_{gp'^{V}}}{I_x}$$

or

$$q_R = q_{g''} + \frac{VQ^{x}_{gp'^{V}}}{I_x} \quad (D)$$

Figure 8

Considering spanwise forces acting upon section p'^{V} d (Fig. 2 and 9), the equilibrium equation gives:

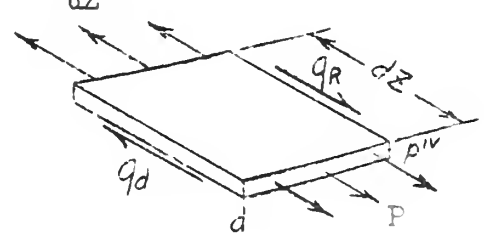

$$q_R - q_d = \left(\frac{dP}{dZ}\right)_{dp'^{V}} = -\frac{VQ^{x}_{dp'^{V}}}{I_x}$$

or

$$q_R = q_d - \frac{VQ^{x}_{dp'^{V}}}{I_x} \quad (4)$$

Figure 9

From equations D and 4:

$$q_{g''} = q_d - \frac{VQ^x_{gp'v}}{I_x} - \frac{VQ^x_{dp'v}}{I_x} = g_d - \frac{VQ^x_{gfed}}{I_x}$$

And equation C becomes:

$$q_{w2} = - q_d + \frac{VQ^x_{gfed}}{I_x} + q_{a'} + \frac{VQ^x_{ag}}{I_x} + \frac{VQ^x_{gp"'}}{I_x}$$

or

$$q_{w2} = q_{a'} - q_d + \frac{VQ^x_{gp"'}}{I_x} + \frac{VQ^x_{agfed}}{I_x} \qquad (5)$$

Considering spanwise forces acting upon section dd'p"' (Fig. 2 and 10), the equilibrium equation gives:

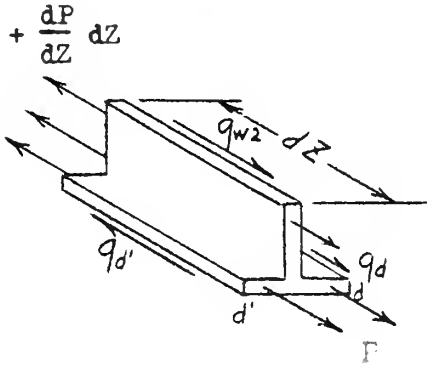

$$q_{w2} + q_d - q_{d'} = \left(\frac{dP}{dZ}\right)_{dp"'} = - \frac{VQ^x_{dp"'}}{I_x} \qquad (E)$$

Figure 10

From equations 5 and E:

$$q_{d'} = q_{a'} + \frac{VQ^x_{dp"'}}{I_x} + \frac{VQ^x_{gp"'}}{I_x} + \frac{VQ^x_{agfed}}{I_x}$$

or

$$q_{d'} = q_{a'} + \frac{VQ^x_{agfedg}}{I_x} \qquad (F)$$

Considering spanwise forces acting upon section d'p^v (Fig. 2 and 11), the equilibrium equation gives:

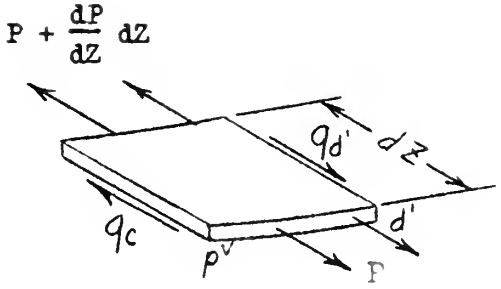

$$q_c - q_{d'} = -\left(\frac{dP}{dZ}\right)_{d'p^V} = \frac{VQ^x_{d'p^V}}{I_x}$$

and from equation F

$$q_c = q_{a'} + \frac{VQ^x_{agfed}}{I_x} + \frac{VQ^x_{d'p^V}}{I_x} \qquad (6)$$

Figure 11

Thus equations one through six represent the spanwise equilibrium equations. These equations involve the unknowns q_n, q_B, q_{w1}, q_{w2}, q_R, q_c, q_a, $q_{a'}$ and q_d. Four additional equations are now obtained by considering the rate of twist of each cell and a moment equation. The moment equation will introduce a new unknown (i.e., the shear center location).

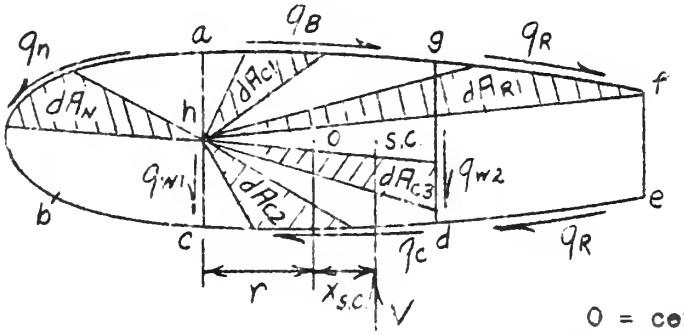

O = centroid
s.c. = shear center

Figure 12

Referring to Figure 12 and taking moments about point h:

$$(G)\quad V(r + x_{s.c.}) + 2\int_{abc} q_n\,dA_N - 2\int_{ag} q_B\,dA_{c1} - 2\int_{gfed} q_R\,dA_{R1} - 2\int_{dc} g_c\,dA_{c2} - 2\int_{gd} q_{w2}\,dA_{c3} = 0$$

Substituting into equation G values of q_n, q_B, q_R, q_c, q_{w2} in terms of q_a, $q_{a'}$, and q_d:

H. $$V(r+x_{s.c.})+2\int_{abc}\left|q_a+\frac{VQ^x_{ap}}{I_x}\right|dA_N-2\int_{ag}\left|q_{a'}+\frac{VQ^x_{a'p''}}{I_x}\right|dA_{c1}-2\int_{gfed}\left|q_d-\frac{VQ^x_{dp'v}}{I_x}\right|dA_{R1}$$

$$-2\int_{dc}\left|q_{a'}+\frac{VQ^x_{agfedg}}{I_x}+\frac{VQ^x_{d'p^v}}{I_x}\right|dA_{c2}-2\int_{gd}\left|-q_d+\frac{VQ^x_{gfed}}{I_x}+q_{a'}+\frac{VQ^x_{ag}}{I_x}+\frac{VQ^x_{gp'''}}{I_x}\right|dA_{c3}$$

Dividing equation H by V and recalling q_a, $q_{a'}$, and q_d are constants:

I. $$(r+x_{s.c.})=-\frac{2q_a}{V}A_n+\frac{2q_{a'}}{V}A_{c1}+\frac{2q_d}{V}A_{R1}+\frac{2q_{a'}}{V}A_{c2}-\frac{2q_d}{V}A_{c3}-\frac{2}{I_x}\int_{abc}Q^x_{ap}dA_n$$

$$+\frac{2}{I_x}\int_{ag}Q^x_{a'p''}dA_{c1}-\frac{2}{I_x}\int_{gfed}Q^x_{dp'v}dA_{R1}+\frac{2}{I_x}\int_{dc}Q^x_{agfedg}dA_{c2}+\frac{2q_{a'}}{V}A_{c3}$$

$$+\frac{2}{I_x}\int_{dc}Q^x_{d'p^v}dA_{c2}+\frac{2}{I_x}\int_{gd}Q^x_{gfed}dA_{c3}+\frac{2}{I_x}\int_{gd}Q^x_{ag}dA_{c3}+\frac{2}{I_x}\int_{gd}Q^x_{gp''}dA_{c3}$$

But $A_{c1}+A_{c2}+A_{c3}=A_c$ (area of center cell)

And $A_{R1}-A_{c3}=A_R$ (area of rear cell)

Hence, equation I becomes:

I. $$(r+x_{s.c.})=-\frac{2q_a}{V}A_N+\frac{2q_{a'}}{V}A_c+\frac{2q_d}{V}A_R+\frac{2}{I_x}Q^x_{agfed}\left[A_{c2}+A_{c3}\right]+\frac{2}{I_x}Q^x_{gd}A_{c2}$$

$$-\frac{2}{I_x}\int_{abc}Q^x_{ap}dA_N+\frac{2}{I_x}\int_{ag}Q^x_{a'p''}dA_{c1}-\frac{2}{I_x}\int_{gfed}Q^x_{dp'v}dA_{R1}+\frac{2}{I_x}\int_{dc}Q^x_{d'p^v}dA_{c2}$$

The equations of the rate of twist for each cell give three additional equations. Note, the rate of twist for each cell is zero since the load is through the shear center.

Front Cell:

J. $$2GA_N\left|\frac{d\theta}{dZ}\right|_{abca}=\int_{abc}q_n\frac{ds}{t}-\int_{ac}q_{w1}\frac{ds}{t}=0$$

Center Cell:

$$K.\quad 2GA_c\left|\frac{d\theta}{dZ}\right|_{acdg} = \int_{ac} q_{w1}\frac{ds}{t} - \int_{cd} q_c\frac{ds}{t} - \int_{gd} q_{w2}\frac{ds}{t} - \int_{ag} q_B\frac{ds}{t} = 0$$

Rear Cell:

$$L.\quad 2GA_R\left|\frac{d\theta}{dZ}\right|_{defg} = \int_{gfed} Q_R\frac{ds}{t} - \int_{gd} q_{w2}\frac{ds}{t} = 0$$

Substituting into equations J, K, and L, the values of q_n, q_{w2}, q_{w1}, q_c, q_B, and q_R in terms of q_a, $q_{a'}$, and q_d.

Front Cell:

$$\int_{abc}\left[q_a + \frac{VQ^x_{ap}}{I_x}\right]\frac{ds}{t} - \int_{ac}\left[-q_a - q_{a'} + \frac{VQ^x_{ap'}}{I_x}\right]\frac{ds}{t} = 0$$

or

$$II.\quad \frac{q_a}{V}\int_{abca}\frac{ds}{t} + \frac{q_{a'}}{V}\int_{ac}\frac{ds}{t} + \frac{1}{I_x}\int_{abc} Q^x_{ap}\frac{ds}{t} - \frac{1}{I_x}\int_{ac} Q^x_{ap'}\frac{ds}{t} = 0$$

Center Cell:

$$\int_{ac}\left[-q_a - q_{a'} + \frac{VQ^x_{ap'}}{I_x}\right]\frac{ds}{t} - \int_{cd}\left[q_{a'} + \frac{VQ^x_{agfedg}}{I_x} + \frac{VQ^x_{d'p^v}}{I_x}\right]\frac{ds}{t}$$

$$- \int_{gd}\left[-q_d + \frac{VQ^x_{gfed}}{I_x} + q_{a'} + \frac{VQ^x_{ag}}{I_x} + \frac{VQ^x_{gp'''}}{I_x}\right]\frac{ds}{t} - \int_{ag}\left[q_{a'} + \frac{VQ^x_{a'p''}}{I_x}\right]\frac{ds}{t} = 0$$

or

$$\text{III.}\quad -\frac{q_a}{V}\int_{ac}\frac{ds}{t}-\frac{q_{a'}}{V}\int_{acdga}\frac{ds}{t}+\frac{q_d}{V}\int_{gd}\frac{ds}{t}-\frac{Q^x_{agfedg}}{I_x}\int_{cd}\frac{ds}{t}-\frac{Q^x_{agfed}}{I_x}\int_{gd}\frac{ds}{t}$$

$$+\frac{1}{I_x}\int_{ac}Q^x_{ap'}\frac{ds}{t}-\frac{1}{I_x}\int_{cd}Q^x_{d'p'\blacktriangledown}\frac{ds}{t}-\frac{1}{I_x}\int_{gd}Q^x_{gp'''}\frac{ds}{t}-\frac{1}{I_x}\int_{ag}Q^x_{a'p''}\frac{ds}{t}=0$$

Rear Cell:

$$\int_{gfed}\left[q_d-\frac{VQ^x_{dp'\blacktriangledown}}{I_x}\right]\frac{ds}{t}-\int_{gd}\left[-q_d+\frac{VQ^x_{gfed}}{I_x}+\frac{VQ^x_{ag}}{I_x}+q_{a'}+\frac{VQ^x_{gp'''}}{I_x}\right]\frac{ds}{t}=0$$

or

$$\text{IV.}\quad \frac{q_d}{V}\int_{gfedg}\frac{ds}{t}-\frac{q_{a'}}{V}\int_{gd}\frac{ds}{t}-\frac{Q^x_{agfed}}{I_x}\int_{gd}\frac{ds}{t}-\frac{1}{I_x}\int_{gfed}Q^x_{dp'\blacktriangledown}\frac{ds}{t}-\frac{1}{I_x}\int_{gd}Q^x_{ag}\frac{ds}{t}=0$$

Thus equations I, II, III, and IV represent four equations with the four unknowns q_a, $q_{a'}$, q_d, and $x_{s.c.}$. Once these equations the desired shear flows can be obtained by use of equations 1 through 6. These equations then, apply to the solution of the shear flow problem involving a structure of three cells, skin fully effective in bending, and the load acting through the shear center.

To the shear flows previously calculated for the load through the shear center, those shear flows due to a torsional load must be added.

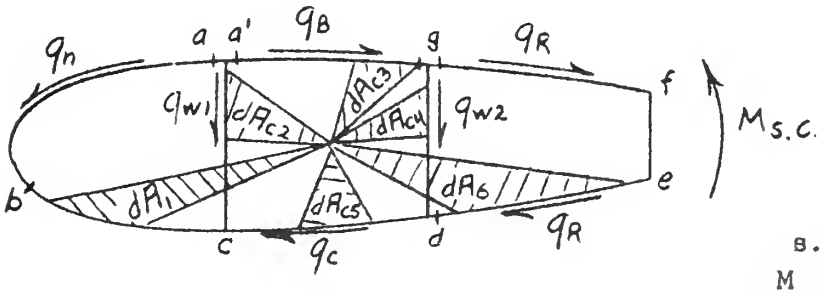

Figure 13

s.c. = Shear Center.
$M_{s.c.}$ = Applied Torsional Moment about Shear Center.

From the previous spanwise equilibrium equations and the fact that $\frac{dp}{dZ} = 0$ for pure torsion the following equations result:

7. $q_n = q_a$

8. $q_{w1} = - q_a - q_{a'}$

9. $q_B = q_{a'}$

10. $q_R = q_d$

11. $Q_{w2} = q_{a'} - q_d$

12. $q_c = q_{a'}$

Taking moments about shear center (Fig. 13) gives:

$$(m) \quad M_{s.c.} + 2\int_{abc} q_N dA_1 + 2\int_{ac} q_{w1} dA_{c2} - 2\int_{a'g} q_B dA_{c3} - 2\int_{cd} q_{w2} A_{c4} - 2\int_{cd} q_c A_{c5} - 2\int_{gfed} q_R dA_6 = 0$$

Substituting into equation (m) the values of q_N, q_{w1}, q_{w2}, q_B, q_c, and q_R in terms of q_a, $q_{a'}$, and q_d gives:

$$M_{s.c.} + 2\int_{abc} q_a dA_1 + 2\int_{ac} (-q_a - q_{a'}) dA_{c2} - 2\int_{ag} q_{a'} dA_{c3}$$

$$-2\int_{gd} (q_{a'} - q_d) dA_{c4} - 2\int_{cd} q_{a'} dA_{c5} - 2\int_{gfed} q_d dA_6 = 0$$

But $A_1 - A_2 = A_N$ (Area of nose cell)

$A_{c2} + A_{c3} + A_{c4} + A_{c5} = A_c$ (Area of center cell)

$A_6 - A_4 = A_R$ (Area of rear cell)

Hence:

$$(V) \quad M_{s.c.} = 2q_{a'} A_c + 2q_d A_R - 2q_a A_N$$

Considering now the rate of twist in each cell and assuming that the rate of twist for each cell is the same gives:

Nose Cell:

$$(n) \qquad 2GA_N \left(\frac{d\theta}{dZ}\right)_{abca} = \int_{abc} q_N \frac{ds}{t} - \int_{ac} q_{w1} \frac{ds}{t}$$

Center Cell:

$$(p) \qquad 2GA_c \left(\frac{d\theta}{dZ}\right)_{acdga} = \int_{ac} q_{w1} \frac{ds}{t} - \int_{cd} q_c \frac{ds}{t} - \int_{gd} q_{w2} \frac{ds}{t} - \int_{ag} q_B \frac{ds}{t}$$

Rear Cell:

$$(q) \qquad 2GA_R \left(\frac{d\theta}{dZ}\right)_{gdefg} = - \int_{gfed} q_R \frac{ds}{t} + \int_{gd} q_{w2} \frac{ds}{t}$$

Substituting into equations (m), (p), and (q), the values of q_N, q_B, q_R, q_{w1}, q_{w2}, and q_c in terms of q_a, $q_{a'}$ and q_d gives:

Nose Cell:

$$(VI) \qquad 2GA_N \left(\frac{d\theta}{dZ}\right)_{abca} = q_a \int_{abca} \frac{ds}{t} + q_{a'} \int_{ac} \frac{ds}{t}$$

Center Cell:

$$(VII) \qquad 2GA_c \left(\frac{d\theta}{dZ}\right)_{acdga} = -q_{a'} \int_{acdga} \frac{ds}{t} - q_a \int_{ac} \frac{ds}{t} + q_d \int_{gd} \frac{ds}{t}$$

Rear Cell:

$$(VIII) \qquad 2GA_R \left(\frac{d\theta}{dZ}\right)_{gdefg} = - q_d \int_{gfedg} \frac{ds}{t} + q_{a'} \int_{gd} \frac{ds}{t}$$

Thus, equations (V), (VI), (VII), and (VIII), represent four equations and four unknowns, q_a, $q_{a'}$, q_d, and $\left(\frac{d\theta}{dZ}\right)$. Once these equations are solved the shear flows due to a torsional load about the shear center

may be determined by use of equations (7) through (12).

Summarizing the equations for the determination of the shear flows in a three cell beam with skin fully effective in bending gives:

A. Equations for Vertical Load Through Shear Center:

$$(I)\quad (r + x_{s.c.}) = -\frac{2q_a A_N}{V} + \frac{2q_{a'} A_c}{V} + \frac{2q_d A_R}{V} + \frac{2}{I_x} Q^x_{agfed}\left[A_{c2} + A_{c3}\right]$$

$$+ \frac{2}{I_x} Q^x_{gd} A_{c2} - \frac{2}{I_x}\int_{abc} Q^x_{ap} dA_N + \frac{2}{I_x}\int_{ag} Q^x_{ap''} dA_{c1} - \frac{2}{I_x}\int_{gfed} Q^x_{dp'v} dA_{R1}$$

$$+ \frac{2}{I_x}\int_{dc} Q^x_{d'pv} dA_{c2}$$

$$(II)\quad \frac{q_a}{V}\int_{abca}\frac{ds}{t} + \frac{q_{a'}}{V}\int_{ac}\frac{ds}{t} + \frac{1}{I_x}\int_{abc} Q^x_{ap}\frac{ds}{t} - \frac{1}{I_x}\int_{ac} Q^x_{ap'}\frac{ds}{t} = 0$$

$$(III)\quad -\frac{q_a}{V}\int_{ac}\frac{ds}{t} - \frac{q_{a'}}{V}\int_{acdga}\frac{ds}{t} + \frac{q_d}{V}\int_{gd}\frac{ds}{t} - Q^x_{agfedg}\int_{cd}\frac{ds}{t}$$

$$- \frac{Q^x_{agfed}}{I_x}\int_{gd}\frac{ds}{t} + \frac{1}{I_x}\int_{ac} Q^x_{ap'}\frac{ds}{t} - \frac{1}{I_x}\int_{cd} Q^x_{d'p'v}\frac{ds}{t}$$

$$- \frac{1}{I_x}\int_{gd} Q^x_{gp'''}\frac{ds}{t} - \frac{1}{I_x}\int_{ag} Q^x_{a'p''}\frac{ds}{t} = 0$$

$$(IV)\quad \frac{q_d}{V}\int_{gfedg}\frac{ds}{t} - \frac{q_{a'}}{V}\int_{gd}\frac{ds}{t} - \frac{Q^x_{agfed}}{I_x}\int_{gd}\frac{ds}{t} - \frac{1}{I_x}\int_{gfed} Q^x_{dp'v}\frac{ds}{t}$$

$$- \frac{1}{I_x}\int_{gd} Q^x_{ag}\frac{ds}{t} = 0$$

(1) $q_n = q_a + VQ^x_{ap}$

(2) $q_{w1} = - q_a - q_{a'} + \frac{VQ^x_{ap'}}{I_x}$

(3) $q_B = q_{a'} + \frac{VQ^x_{a'p''}}{I_x}$

(4) $q_R = q_d - \frac{VQ^x_{dp'''}}{I_x}$

(5) $q_{w2} = q_{a'} - q_d + \frac{VQ^x_{agfed}}{I_x} + \frac{VQ^x_{gp'''}}{I_x}$

(6) $q_c = q_{a'} + \frac{VQ^x_{agfedg}}{I_x} + \frac{VQ^x_{d'p'''}}{I_x}$

B. Equations for Torsional Load:

(V) $M_{s.c.} = 2q_{a'}A_c + 2q_dA_R - 2q_aA_N$

(VI) $2GA_N\left(\frac{d\theta}{dZ}\right)_{abca} = q_a\int_{abca}\frac{ds}{t} + q_{a'}\int_{ac}\frac{ds}{t}$

(VII) $2GA_c\left(\frac{d\theta}{dZ}\right)_{acdga} = - q_{a'}\int_{acdga}\frac{ds}{t} - q_a\int_{ac}\frac{ds}{t} + q_d\int_{gd}\frac{ds}{t}$

(VIII) $2GA_R\left(\frac{d\theta}{dZ}\right)_{gdefg} = -q_d\int_{gfedg}\frac{ds}{t} + q_{a'}\int_{gd}\frac{ds}{t}$

(7) $q_n = q_a$

(8) $q_{w1} = -q_a - q_{a'}$

(9) $q_B = q_{a'}$

(10) $q_R = q_d$

(11) $q_{w2} = q_{a'} - q_d$

(12) $q_c = q_{a'}$

(13) $\left|\frac{d\theta}{dZ}\right|_{abca} = \left|\frac{d\theta}{dZ}\right|_{acdga} = \left|\frac{d\theta}{dZ}\right|_{gdefg}$

Referring to the above summary of equations, the resulting shear flows for pure torsion are of constant value between any two successive structural junctions, while the shear flows due to bending vary between such junction points. The maximum and minimum values of these shear flows can of course be obtained by differentiating the shear flow expression with respect to the parameter defining the amount of area of the appropriate section.

The procedure employed in the analysis of the subject three cell beam is applicable to a 'n' cell beam (for n > 2) where,

$3n - 2$ = number of unknowns (i.e., shear flows and shear center location).

n = number of equations available from the rate of twist of each cell.

1 = moment equation.

Thus:

$(3n - 2) - (n - 1) = 2n - 3$ = number of points at which the shear value is assumed.

Previously it was shown that when considering the principal axes

then $\left|\frac{dP}{dZ}\right|_{ap} = -\frac{VQ^x_{ap}}{I_x}$

If the axes are not principal axes and in addition the load is acting in any given direction then

$$P = \int_{ap} \left(\frac{M_x I_{xy} - M_y I_x}{I_x I_y - I_{xy}^2} x + \frac{M_y I_{xy} - M_x I_y}{I_x I_y - I_{xy}^2} y \right) dA$$

$$= \frac{M_x I_{xy} - M_y I_x}{I_x I_y - I_{xy}^2} \int_{ap} x\,dA + \frac{M_y I_{xy} - M_x I_y}{I_x I_y - I_{xy}^2} \int_{ap} y\,dA$$

$$= \frac{M_x I_{xy} - M_y I_x}{I_x I_y - I_{xy}^2} Q^y_{ap} + \frac{M_y I_{xy} - M_x I_y}{I_x I_y - I_{xy}^2} Q^x_{ap}$$

$$P = \frac{1}{I_x I_y - I_{xy}^2} \left[M_x (I_{xy} Q^y_{ap} - I_y Q^x_{ap}) + M_y (I_{xy} Q^x_{ap} - I_x Q^y_{ap}) \right]$$

$$\text{(IX)} \quad \frac{dP}{dZ} = \frac{1}{I_x I_y - I_{xy}^2} \left[V_y (I_{xy} Q^y_{ap} - I_y Q^x_{ap}) + V_x (I_{xy} Q^x_{ap} - I_x Q^y_{ap}) \right.$$

$$\left. + M_x \frac{d}{dZ} \left(\frac{I_{xy} Q^y_{ap} - I_y Q^x_{ap}}{I_x I_y - I_{xy}^2} \right) + M_y \frac{d}{dZ} \left(\frac{I_{xy} Q^x_{ap} - I_x Q^y_{ap}}{I_x I_y - I_{xy}^2} \right) \right]$$

Thus the algebra now involved is very cumbersum, and a practical analysis would require some assumptions or approximations wherein this difficulty could be overcome. For example, in the procedure employed herein it was assumed the wing or beam had no taper, hence, the last two terms of equation (IX) each equals zero. Also principal axes were used, thus I_{xy} equals zero, and only a vertical load (i.e., perpendicular to the x axis) was considered. These qualifications reduce equation (IX) to

$$\left(\frac{dP}{dZ} \right)_{ap} = \frac{V Q^x_{ap}}{I_x}$$

Also worthy of note, is that the shear center location as derived herein is different than that location as obtained from the analysis where the skin is considered either non-effective or partially effective in bending.

PART II

STRESS ANALYSIS AND STATIC TEST OF A MODEL WING

PART II

STRESS ANALYSIS AND STATIC TEST OF A MODEL WING

This part of the report includes the stress analysis and static test of a three cell model wing. The wing was constructed from .072-24ST aluminum sheet, with six foot span, twelve inch chord, and circular arc airfoil shape. As far as the stress analysis is concerned, those equations developed in Part I could be applied directly, however, due to the symmetry of the wing, the shear flow equations are somewhat simpler than those of Part I, hence, a separate stress analysis for the wing using the previous procedure is included. The initial sections of Part II are devoted to this stress analysis and the actual static test follows.

Geometric Properties of Model Wing

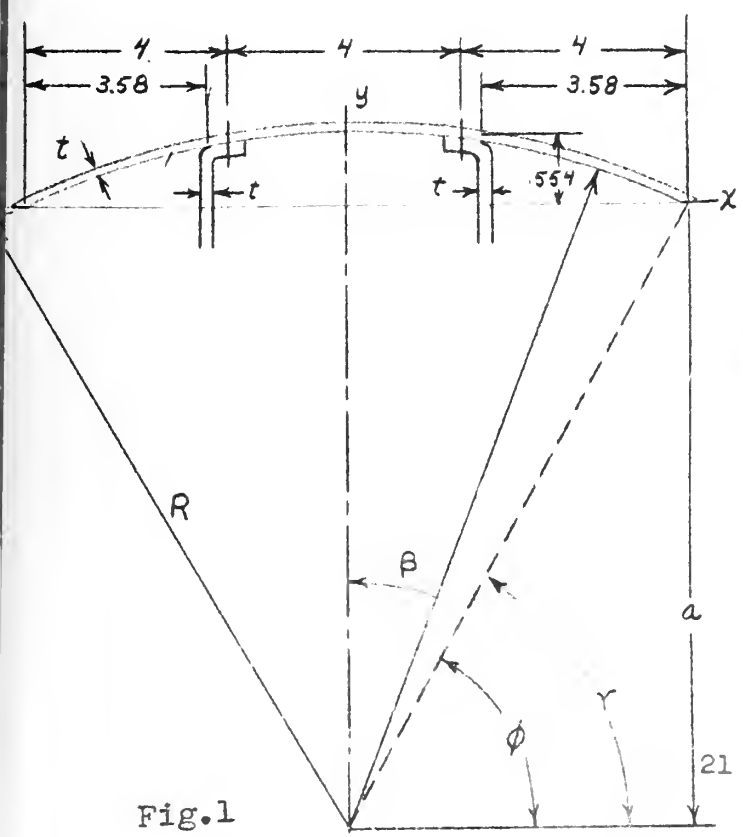

Fig.1

Due to symmetry about chord line only upper half of wing need be considered.

$(y+a)^2 + x^2 = R^2$

$a+x = o, y = .64$

$.64+a = R$

$a = R - .64 = 27.805"$

$\sin \gamma = \frac{a}{R} = \frac{27.805}{28.445}$

$= .9775$

$\gamma = 1.3585$ rad.

$t = .072"$
$R = 28.448"$
$c = 12"$
$a = 27.805"$
$R^2 = 809.118$ sq.in.
$a^2 = 773.118$ sq.in.
$\gamma = 1.3585$ rad.
$\sin \gamma = .9775$
$aR = 790.9132$

Moment of Inertia (I_{xx}):

$$I_{x\ skin} = 4\int_{\gamma}^{\pi/2} y^2\, dA \qquad dA = Rtd\,\phi \qquad R\sin\phi = y + a$$

$$I_{x\ skin} = 4\int_{\gamma}^{\pi/2} (R\sin\phi - a)^2\, Rtd\,\phi$$

$$= 4Rt\left[\frac{R^2\phi}{2} - \frac{R^2}{4}\sin 2\phi + 2aR\cos\phi + a^2\phi\right]_{1.3585}^{\pi/2}$$

$$= 8.192\left\{404.559\left[1.570796 - 1.3585\right] - 202.279\left[0 - \sin 2.7170\right] + 790.9132\times 2\left[0 - \cos 1.3585\right] + 773.118\times .212296\right\}$$

$$= 8.192\left\{404.554\times .212296 + 202.279\times .411949 + 158.18264\times [-.21070] + 773.118\times .212296\right\}$$

$$= 8.192\left\{85.885 + 83.32863 - 333.29082 + 164.1298\right\}$$

$$= 8.192\times .05261 = .4309895\ \text{in.}^4$$

$$\underline{I_{x\ skin} = .4309895\ \text{in.}^4}$$

$$I_{webs} = 2\times\frac{bh^3}{12} = \frac{.072\times .96^3}{6} = .012\times .875136 = .0105016$$

$$I_{flanges} = 4\left[\frac{bh^3}{12} + Ad^2\right] = 4\left[\frac{.6\times .072^3}{12} + .6\times .072\times .475^2\right]$$

$$= .0097648$$

$$\underline{\underline{I_{total} = .44149\ \text{in.}^4}}$$

Geometric Properties of Model Wing:

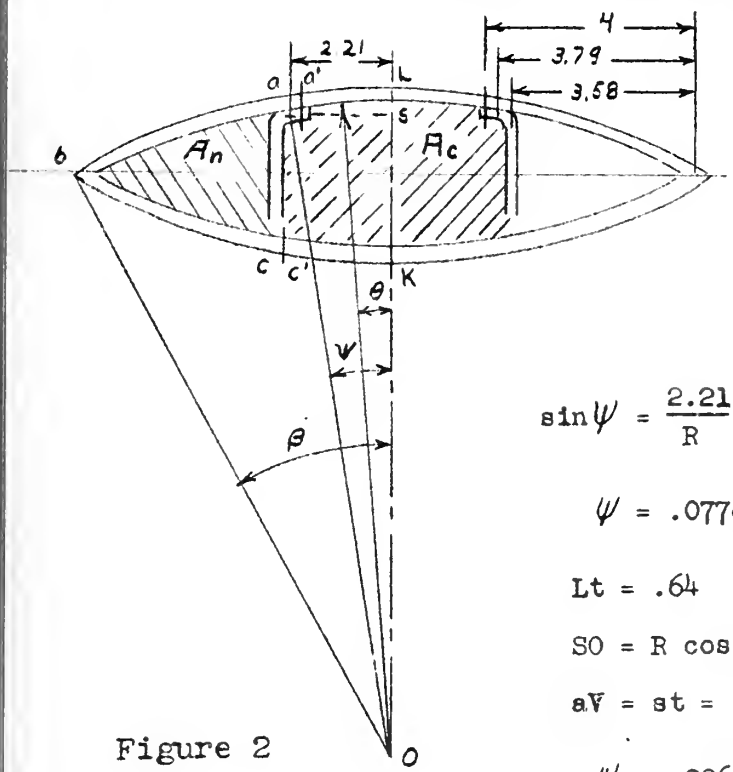

Figure 2

Note: The rivet line for the spar is 4 inches from trailing edge. The web location is 3.58 inches from trailing edge. For purposes of analysis the spar loading is assumed to transfer to the skin at some point between the rivet line and web line (e.g., 3.79" from t.e.).

$$\sin\psi = \frac{2.21}{R} = \frac{2.21}{28.445} = .0777 \qquad \sin\beta = \frac{6}{R} = \frac{6}{28.445} = .211$$

$$\psi = .0778 \text{ rad.} \qquad \beta = .2126 \text{ rad.}$$

$$Lt = .64$$

$$SO = R\cos\psi = 28.445 \quad .99698 = 28.3591$$

$$aV = st = .5541"$$

$$\cos\psi = .99698 \qquad \cos\beta = .9775$$

$$\int_{La'} ds = \int_0^{\psi} Rd\theta = R(\psi - 0) = 28.445 \quad .0778 = 2.215"$$

$$\int_{ab} ds = \int_{\psi}^{\beta} Rd\theta = R(\beta - \psi) = 28.445\ (.2116 - .0778) = 3.802"$$

$$\int_{abc} ds = 2\int_{ab} ds = 7.604"$$

$$\int_{ga'} ds = 2\int_{La'} ds = 4.430"$$

$$\int_{ac} ds = 2\int_0^{.55} dy = 1.10"$$

$$\frac{1}{4}A_c: \quad \frac{\text{Area "aOL"}}{R^2} = \frac{\psi}{2\pi} \text{ or } \quad \text{Area 'aOL'} = \frac{.0778 \times 809.118}{2} = 31.47459$$

Area "aos" = $\frac{1}{2} \times 28.3591 \times 2.21 = 31.3368$

$\frac{1}{4} A_c = 2.21 \times .55 + 31.4759 - 31.3368 = 1.3532$ sq.in.

$A_c = 5.4128$ sq. in.

$\frac{1}{2} A_n$ = Area "boL" - $\frac{1}{4} A_c$ - "bot"

$\frac{\text{Area 'boL'}}{R^2} = \frac{\beta}{2\pi}$ Area "boL" = $\frac{.2126 \times 809.118}{2} = 86.00924$

Area "bot" = $\frac{1}{2} \times 6 \times a = 3 \times 27.805 = 83.415$

$\frac{1}{2} A_n = 86.00924 - 1.3532 - 83.418 = 1.2407$

$A_n = 2.4814$ sq. in.

Calculation of Moment of Areas: (Refer to Fig. 6)

$$\int_{La'} Q^x_{Lp''}\, ds: \quad Q^x_{Lp''} = \int_0^\theta y\, Rt\, d\theta = \int_0^\theta Rt\,(R\cos\theta - a)\, d\theta$$

$$= Rt\left[R\sin\theta - a\theta\right]$$

$$\int_{La'} Q^x_{Lp''}\, ds = \int_0^{\psi=.0778} R^2 t\left[R\sin\theta - a\theta\right] d\theta$$

$$= R^2 t\left\{-R\cos\theta - \frac{a\theta^2}{2}\right\}_0^{.0778}$$

$$= 809.118 \times .072\left\{-28.445(.99698 - 1) - \frac{27.805 \quad .0778^2}{2}\right\}$$

$$= 58.25649\left\{.0859039 - .0841465\right\}$$

$$= .10237995$$

$$\int_{ab} Q^x_{ap}\, ds: \quad Q^x_{ap} = \int_{\psi}^{\theta} Rt\, y d\theta = \int_{\psi}^{\theta} Rt\,(R\cos\theta - a)\, d\theta$$

$$= Rt\left[R(\sin\theta - \sin\psi) + a(\psi - \theta)\right]$$

$$\int_{ab} Q^x_{ap}\, ds = \int_{\psi}^{\beta} R^2 t\left[R(\sin\theta - \sin\psi) + a(\psi - \theta)\right] d\theta$$

$$= R^2 t\left[-R\cos\theta - R\theta\sin \quad + a \quad \theta - \frac{a\theta^2}{2}\right]_{\psi}^{\beta}$$

$$= R^2 t\left[-R(\cos\beta - \cos\psi) - R(\beta - \psi)\sin\psi + a\psi\beta - \frac{a\psi^2}{2} - \frac{a\beta^2}{2}\right]$$

$$= 58.25649\left\{-R(-.01948) - R(.1348)\times.0777 + a\times.0778\times.2126 - \frac{a(.0778)^2}{2} - \frac{a(.2126)^2}{2}\right\}$$

$$= 58.25649\left\{.5541086 - .29793179 + .45990248 - .0841496 - .6283531\right\}$$

$$= 58.25649 \times .00357659$$

$$= .208359579$$

$$\int_{ac} Q^x_{ap'}\, ds: \quad Q^x_{ap'} = \int_{y}^{h=.5541} yt\, dy = \frac{h^2 t}{2} - \frac{y^2 t}{2} = \frac{t}{2}(h^2 - y^2)$$

$$\int_{ac} Q^x_{ap'}\, ds = 2\int_{0}^{h=.5541} \frac{t}{2}(h^2 - y^2)\, dy = t\left[h^2 y - y^3/3\right]_0^h$$

$$= t\left[h^3 - \frac{h^3}{3}\right] = \frac{2h^3 t}{3}$$

$$= \frac{2\times.5541^3\times.072}{3} = .00816592$$

$$\int_{ac} Q^{x}_{a'L}\, ds \qquad Q^{x}_{a'L} = \int_{0}^{\psi=.0778} yRtd\theta = \int_{0}^{\psi} Rt(R\cos\theta - a)\, d\theta$$

$$= Rt\left[R\sin\theta - a\theta\right]_{0}^{.0778}$$

$$= 2.04804\left[28.445 \times .0777 - 27.805 \times .0778\right]$$

$$= 2.04804\left[2.2101765 - 2.163229\right]$$

$$= .096147456$$

$$\int_{ac} Q^{x}_{a'L}\, ds = .09614745 \times 1.10$$

$$= .10576219$$

Geometric Properties of Wing

(Strain Gage Locations)

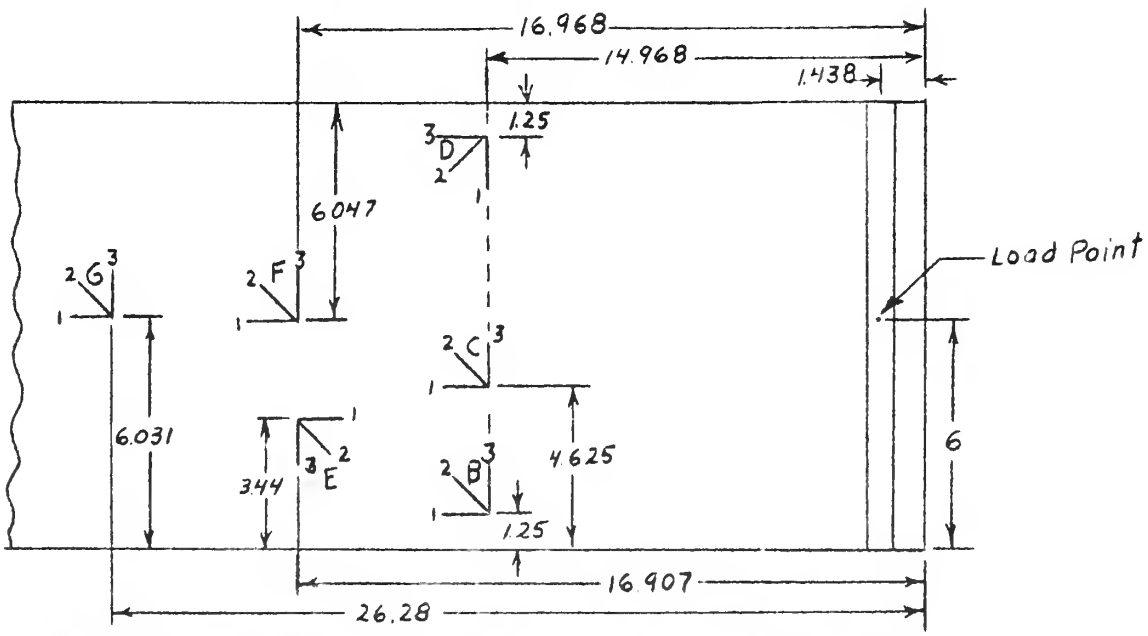

Fig. 3 Planform of wing showing strain gauge locations:

Referring to Fig. 3, the strain gauge locations are those actually used in the static test. They are introduced here in order to analytically determine the shear stresses at these locations.

Stress Analysis for Vertical Load Through Shear Center

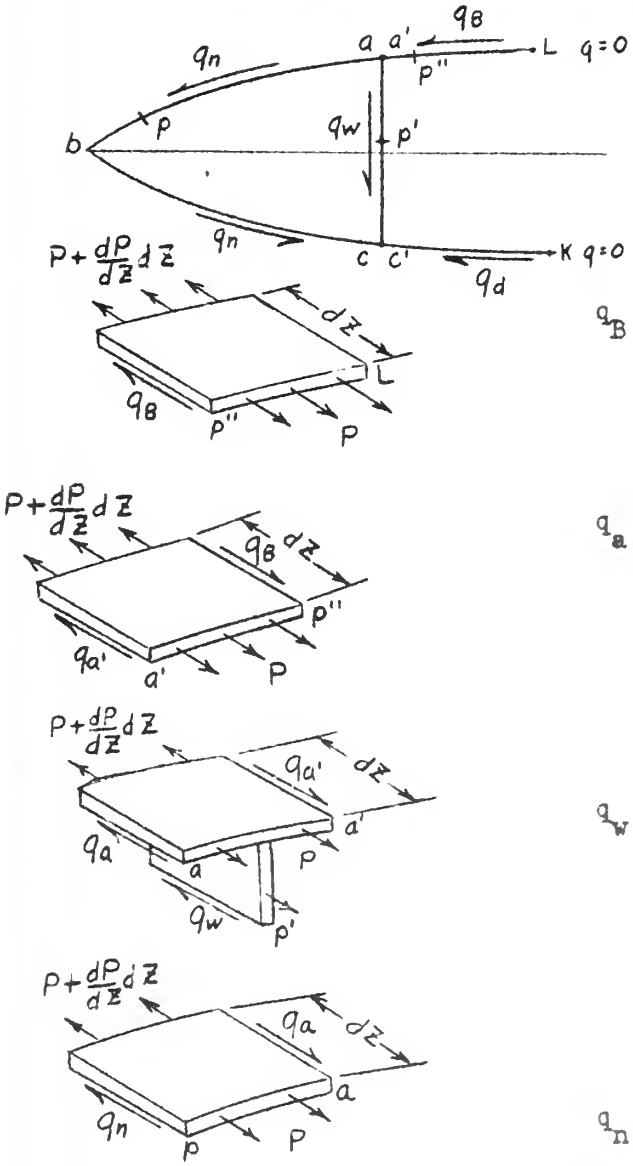

$$q_B = \frac{VQ^x_{Lp''}}{I_x} \qquad (1)$$

$$q_{a'} - q_B = \frac{VQ^x_{a'p''}}{I_x}, \quad q_{a'} = \frac{VQ^x_{a'p''}}{I_x} + \frac{VQ^x_{Lp''}}{I_x} = \frac{VQ^x_{a'L}}{I_x} \qquad (2)$$

$$q_w + q_a - q_{a'} = \frac{VQ^x_{ap'}}{I_x}, \quad q_w = -q_a + \frac{VQ^x_{ap'}}{I_x} + \frac{VQ^x_{a'L}}{I_x} \qquad (3)$$

$$q_n - q_a = \frac{VQ^x_{ap}}{I_x} \qquad (4)$$

Fig. 4

Twist of Nose Cell:

$$\int_{abc} q_n \frac{ds}{t} - \int_{ac} q_w \frac{ds}{t} = 0 \qquad (5)$$

$$\int_{abc} \left(q_a + \frac{VQ^x_{ap}}{I_x}\right) ds - \int_{ac} \left[-q_a + \frac{VQ^x_{ap'}}{I_x} + \frac{VQ^x_{a'L}}{I_x}\right] ds = 0$$

$$q_a \int_{abc} ds + q_a \int_{ac} ds + \int_{abc} \frac{VQ^x_{ap}}{I_x} ds - \int_{ac} \left[\frac{VQ^x_{ap'}}{I_x} + \frac{VQ^x_{a'L}}{I_x}\right] ds = 0$$

$$2q_a \int_{ab} ds + q_a \int_{ac} ds + \frac{2V}{I_x} \int_{ab} Q^x_{ap} ds - \frac{V}{I_x} \int_{ac} (Q^x_{ap'} + Q_{a'L}) ds = 0$$

$$2q_a(3.802) + q_a(1.10) + \frac{2V}{I_x}(.2083596) - \frac{V}{I_x}(.0081659 + .10576219) = 0$$

$$8.704\, q_a + \frac{V}{I_x}\left[.4167192 - .1139281\right] = 0$$

$$8.704\, q_a + .3027911 \frac{V}{I_x} = 0$$

$$q_a = -.03479 \frac{V}{I_x}$$

$$q_a = -.0788\ V$$

$$q_{a'} = \frac{VQ^x_{a'L}}{I_x} \qquad Q^x_{a'L} = \int_0^{\psi} Rt\,(R\cos\theta - a)\, d\theta = Rt\left[R\sin\psi - a\psi\right]$$

$$= 2.04804\left[28.445 \times .0777 - 27.805 \times .0778\right]$$

$$= 2.04804\left[2.210176 - 2.163229\right]$$

$$= .0469475$$

$$q_{a'} = \frac{.0469475}{.44149}\ V$$

$$q_{a'} = .1063\ V$$

Strain Gage C.

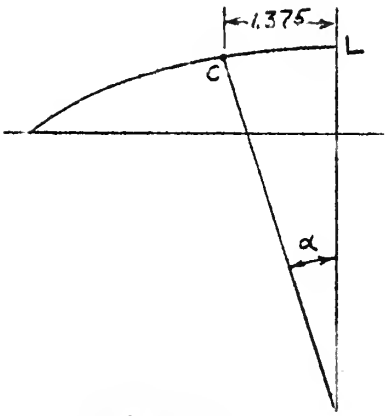

Figure 5

$$\sin\alpha = \frac{1.375}{R} = \frac{1.375}{28.445} = .0483$$

$$\alpha = .0484 \text{ rad.}$$

$$Q^x_{Lc} = Q^x_{Lp''} \text{ when } \theta = \alpha = .0484$$

$$Q^x_{Lp''} = Rt\left[R\sin\theta - a\theta\right]$$

$$Q^x_{Lc} = 2.04804\left[28.445 \times .0483 - 27.805 \times .0484\right]$$

$$= 2.04804\left[1.37389 - 1.343762\right]$$

$$= 2.04804 \times .03013$$

$$= .06171$$

$$q\Big]_{\text{gage c}} = \frac{VQ^x_{Lc}}{I_x}$$

$$\tau_c = .13977\ V$$

$$\tau_c = \frac{q_c}{t} V = 1.9412\ V$$

Strain Gage B.

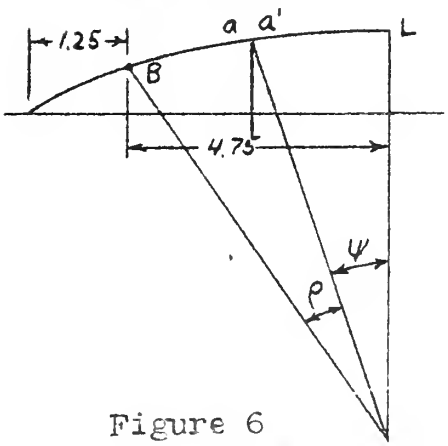

Figure 6

From eqt. (4) p a.

$$q_n - q_a = \frac{VQ^x_{ap}}{I_x}$$

$$\text{or } q_B - q_a = \frac{VQ^x_{aB}}{I_x}$$

$$\sin\rho = \frac{4.75}{R} = \frac{4.75}{28.445} = .1669$$

$$\rho = .1679$$

$$Q^x_{aB} = \int_{\psi}^{\rho} Rt\left[R\cos\theta - a\right] d\theta$$

$$= Rt\left[R(\sin\rho - \sin\psi) - a\rho + a\psi\right]$$

$$= 2.04804\left[28.445(.1679 - .0777) - a(.1679 - .0778)\right]$$

$$= 2.04804\left[2.565739 - 2.5052305\right]$$

$$= 2.04804 \times .06051 = .1239269$$

$$q_B = q_a + \frac{VQ^x_{aB}}{I_x} = -.0788V + .2807V$$

$$q_B = .2019V \qquad \tau_B = 2.804V$$

Hence, the shear stresses as analytically determined at strain gauge locations B and C, due to a vertical load through the shear center of the wing are:

At location B: $\tau_B = 2.804\ V$ p.s.i.

At location C: $\tau_C = 1.941\ V$ p.s.i.

where V = applied load.

Stress Analysis for Moment about Shear Center

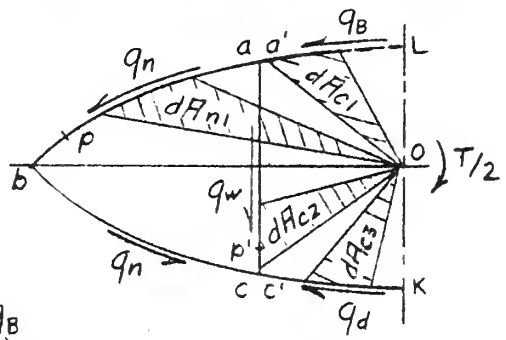

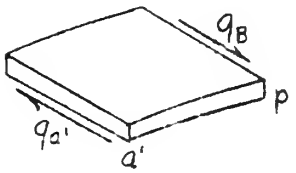

$$q_{a'} - q_B = 0, \quad q_a = q_B \qquad (a)$$

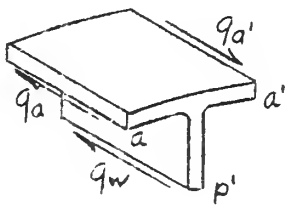

$$q_a + q_w - q_{a'} = 0 \quad q_w = q_{a'} - q_a \qquad (b)$$

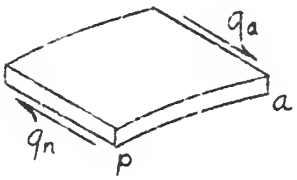

$$q_n = q_a \qquad (c)$$

Due to symmetry $q_s = -q_B$ (d)

Figure 7

Taking Moments about Point O:

$$2\int_{La'} q_B\, dA_{c1} + 2\int_{abc} q_n\, dA_{n1} + 2\int_{ac} q_w\, dA_{c2} - 2\int_{c'k} q_d\, dA_{c3} = \frac{T}{2}$$

$$q_{a'}\int_{La'} dA_{c1} + q_a\int_{abc} dA_{n1} + (q_{a'} - q_a)\int_{ac} dA_{c2} + q_{a'}\int_{a'k} dA_{c3} = \frac{T}{4}$$

$$q_{a'}\left[\int_{La'} dA_{c1} + \int_{ac} dA_{c2} + \int_{c'k} dA_{c3}\right] + q_a\left[\int_{abc} dA_{n1} - \int_{ac} dA_{c2}\right] = \frac{T}{4}$$

(5) $q_{a'} A_c + q_a A_n = \frac{T}{4}$ where $A_c = \frac{1}{2}$ area of center cell

A_n = area of nose cell.

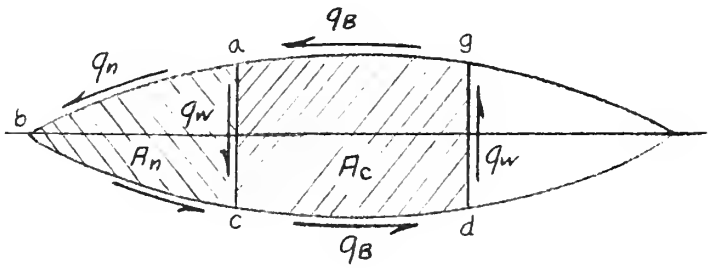

Figure 8

Twist of Nose Cell:

$$2GA_n\left|\frac{d\theta}{dZ}\right| = \int_{abc} q_n \frac{ds}{t} - \int_{ac} q_w \frac{ds}{t}$$

$$= q_a\int_{abc} \frac{ds}{t} - (q_{a'} - q_a)\int_{ac} \frac{ds}{t}$$

$$= \frac{q_a}{t}\int_{abc} ds + \int_{ac} ds - \frac{q_{a'}}{t}\int_{ac} ds$$

$$\frac{d\theta}{dZ} = \frac{1}{2GA_n t}\left[q_a\int_{abc} ds + q_a\int_{ac} ds - q_{a'}\int_{ac} ds\right]$$

Twist of Center Cell:

$$2GA_c\left|\frac{d\theta}{dZ}\right| = \int_{ga} q_B \frac{ds}{t} + \int_{ac} q_w \frac{ds}{t} + \int_{cd} q_B \frac{ds}{t} + \int_{dg} q_w \frac{ds}{t}$$

$$= \frac{2}{t}\int_{ga} q_B ds + \frac{2}{t}\int_{ac} q_w ds$$

$$= \frac{2}{t}\int_{ga} q_a' ds + \frac{2}{t}\int_{ac} (q_a' - q_a)\, ds$$

$$= \frac{2}{t} q_a' \left[\int_{ga} ds + \int_{ac} ds\right] - \frac{2q_a}{t}\int_{ac} ds$$

$$\frac{d\theta}{dZ} = \frac{1}{GA_c t}\left[q_a' \int_{ga} ds + q_a' \int_{ac} ds - q_a \int_{ac} ds\right]$$

$$\left.\frac{d\theta}{dZ}\right|_{\substack{\text{nose}\\ \text{cell}}} = \left.\frac{d\theta}{dZ}\right|_{\substack{\text{center}\\ \text{cell}}}$$

$$\frac{1}{2A_n}\left[q_a(7.604 + 1.10) - q_a' \times 1.10\right] = \frac{1}{A_c}\left[q_a'(4.430 + 1.10) - q_a \times 1.10\right]$$

$$\frac{5.4128}{4 \times 2.4814}(8.704\, q_a - 1.10\, q_a') = 5.530\, q_a' - 1.10\, q_a$$

$$4.74655\, q_a - .599863\, q_a' = 5.530\, q_a' - 1.10\, q_a$$

$$5.84655\, q_a = 6.12986\, q_a'$$

$$(6) \qquad q_a = 1.0484\, q_a'$$

From eqt. (5) $\quad \frac{5.4128}{2} q_a' + 2.4814 \times 1.0484 q_a' = \frac{T}{4}$

$$5.30789\, q_a' = \frac{T}{4} \qquad q_a' = .0471\, T \qquad \tau_a' = .6542\, T$$

$q_a = 1.0484\ q_{a'} = 1.0484 \times .0471\ T$

$q_a = .04938\ T \qquad \tau_a = .6858\ T$

Hence, the shear stresses as analytically determined at strain gauge locations B and C, due to a moment about the shear center of the wing are:

At location B: $\tau_B = .6858\ T$ p.s.i.

At location C: $\tau_C = .6542\ T$ p.s.i.

where T = applied moment.

EQUIPMENT AND PROCEDURE

The geometry and material of the model wing has been discussed previously. An attempt was made to test the wing in pure bending (i.e., no torsion) and in pure torsion. Six SR-4 strain gages were mounted on the wing and an additional one installed upon a small sheet of 24ST aluminum for temperature correction purposes. (See Fig. 3 for strain gage locations.) The rig by which the bending test was conducted is shown in Fig. 9. Referring to Fig. 9, the load was applied by adjusting the turnbuckle which appears on the right. The amount of load was determined by a previously calibrated dynamometer installed just below the turnbuckle. Strain gage readings were obtained at several load values, varying from zero to 437 pounds. (See Tables I and II at end of this report.)

Following the bending test the wing was tested in torsion. The rig used here is shown in Figs. 10 and 11. Referring to Fig. 10, the load was applied by a hydraulic jack and amount of load determined by use of the dynamometer used in the bending test. Not apparent from Figs. 10 and 11 is the balance scheme used, wherein a cable was attached to the free end of the wing and loaded with sand bags such that the wing was not subjected to bending due to its own weight. Strain gage readings were obtained at several torsional load values, varying from zero to over 6000 in.lbs. (See Table III at the end of this report.)

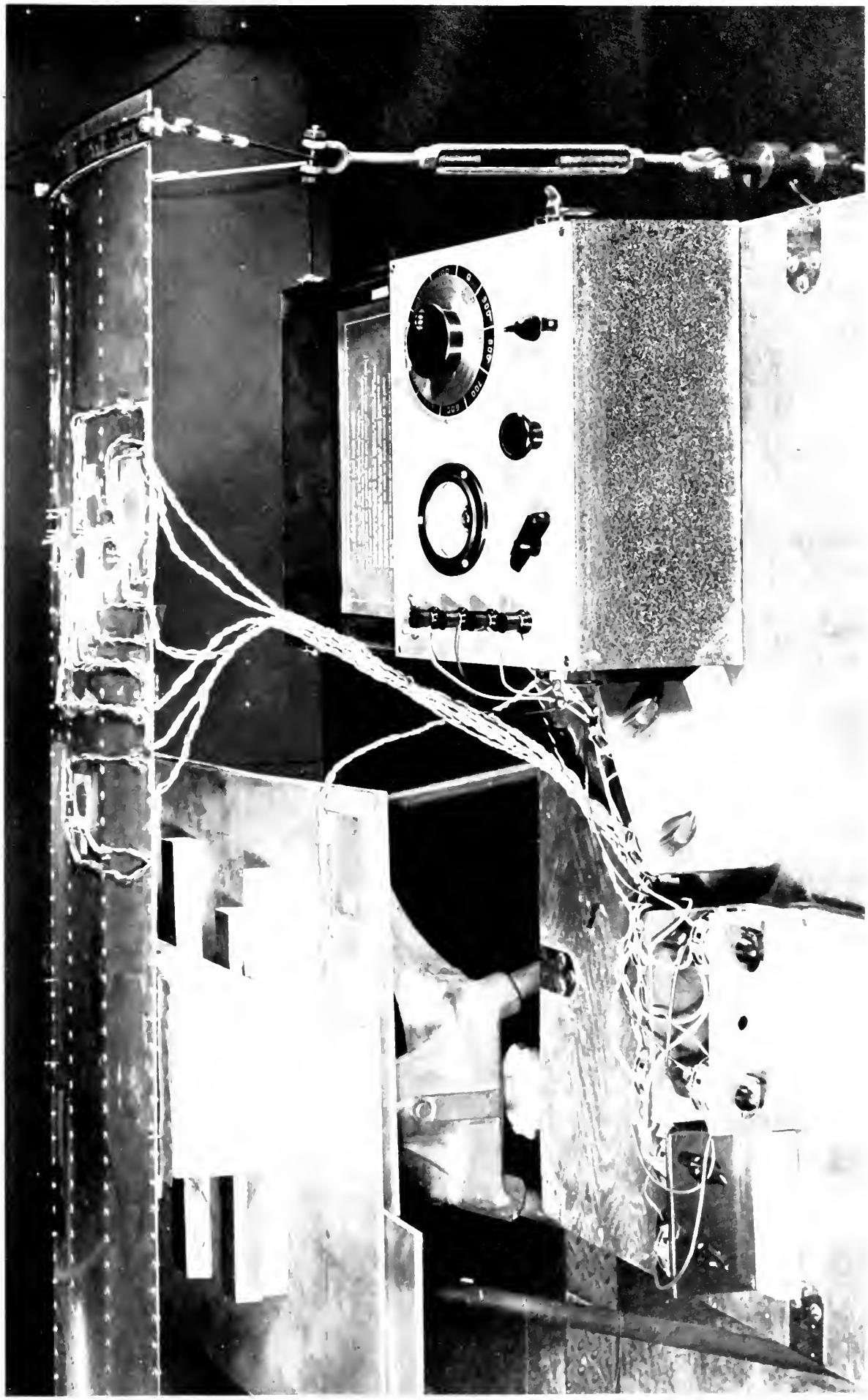

Fig.9. Bending Test

ig.10. Torsion Test

RESULTS AND DISCUSSION

From the resulting test data (i.e , Tables I, II, and III) Mohr stress circles were drawn for each strain gage, corresponding to V = 400 pounds in the bending test and T = 6230 inch pounds in the torsion test. This was done somewhat as a preliminary check (i.e., a comparison between experimental shear stress values with those calculated previously). Considerable disagreement in results was indicated at this point. It appeared that perhaps the bending test actually introduced some torsional moment upon the wing and similarly the torsion test introduced some bending upon the wing. Having sufficient data, it was possible to attempt to separate the torsional shear stresses from the bending shear stresses in both the bending and torsion tests. This was done and the experimental results were compensated for accordingly. However, there was still considerable disagreement between the experimental and analytical results. The stress circles are not included in this report since their only apparent value was to show considerable disagreement between the experimental and analytical results.

In view of this disagreement in results, the next logical approach appeared to be an attempt at determining the reliability of the experimental strains. Figure 12 is a plot of load vs. strain from strain gages C, B, and E. From this plot it is apparent that there was no over-all linearity of stress-load variation as predicted by Hookes Law. The causes leading to this non-linearity between stress and load might be attributed to the inherent random error in the strain determination, instability of the structure wherein the slippage at the riveted joints causes portions of the structure to load or unload in some unpredictable fashion, error

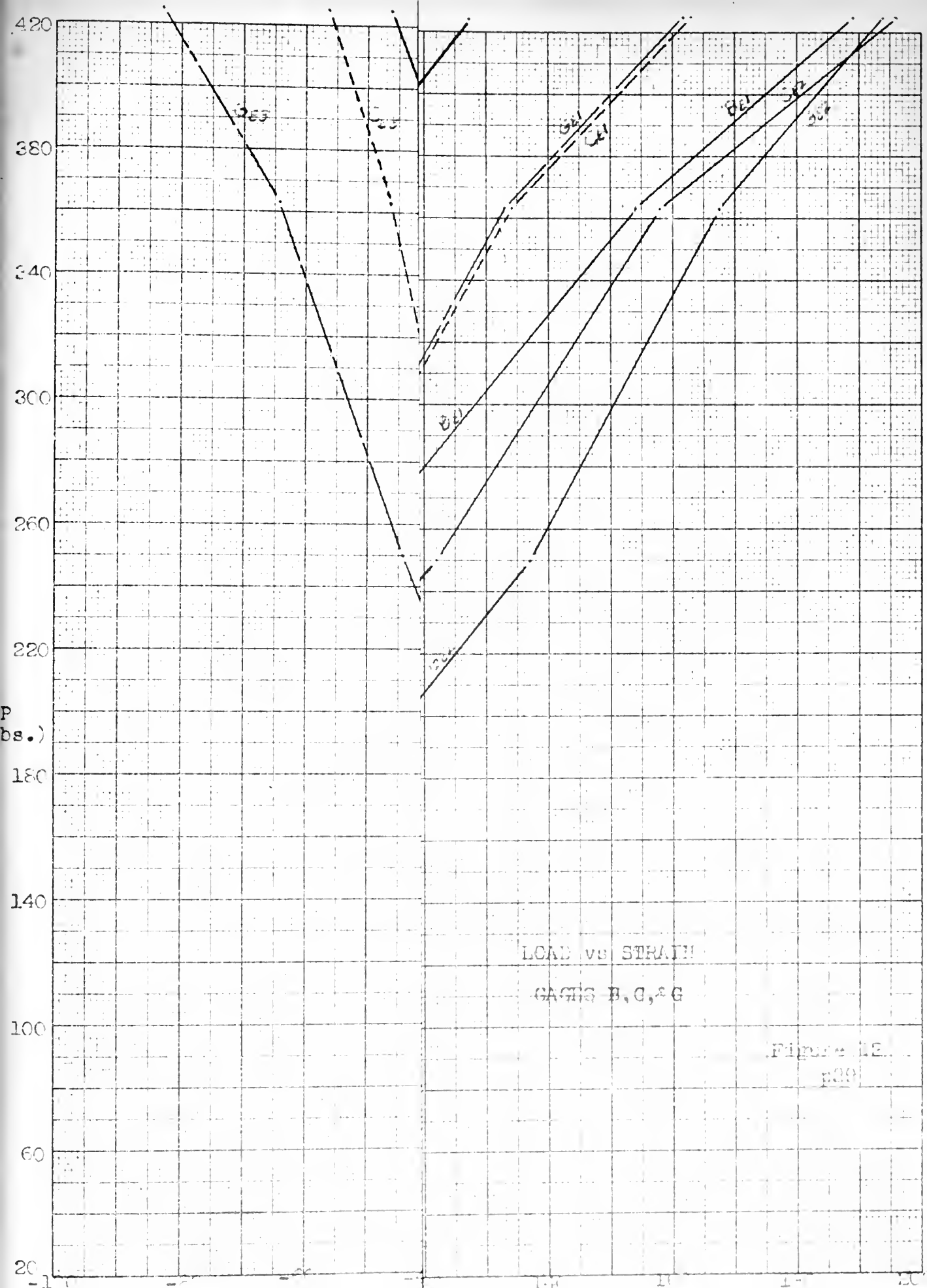

LOAD vs STRAIN

GAGES B, C, & G

Figure 12

P (lbs.)

420
380
340
300
260
220
180
140
100
60
20

-100 -80 -60 -40 -20 0 20 40 80 100 120 140 160 180 200
-20 -16 -12 -8 -4 0 4 8 16 20 24 28 32 36 40
-50 -40 -30 -20 -10 0 10 20 40 50 60 70 80 90 100

STRAIN ($\times 10^{-5}$)

LOAD vs STRAIN

GAGES B, C, & G

Figure 12

P30

due to local effects of the rivets (i.e., St. Venant principle), scale factor of the model and limitations of the strain gages.

In discussion each of the above sources of error, the results of Figure 12 indicates the inherent random error of the strain determinations was of minor importance, since the irregularities in the strain are of much larger magnitude than those attributable to random error, where it is known that the strain-meter readings as such, are at least accurate to within plus or minus one-half microinch. Error in the load determination may be ruled out since such errors would need be in order of magnitude of plus fifty pounds at some points and minus fifty pounds at other points.

Errors due to scale factor of the model and limitations of strain gages appear as possibly large, when considering that the magnitude of shear stresses is quite low and the shear stress values so critically dependent upon the precise location of the strain gages. For example, in bending with the applied load equal to approximately four hundred pounds the shear stress in the skin over the center cell of the wing varies from zero at the center of the panel to approximately eight hundred pounds per square inch at the web skin junction. Thus the shear stress varies from zero to eight hundred pounds per square inch over a distance of about two inches, hence, the requirement for precise location of the strain gages. In this respect it should be noted that when using a strain rosette the strain readings are assumed to represent those strains at the intersection of the gage axes on the strain gage (Fig. 13).

Figure 13 is a full scale diagrammatic representation of the strain gages used in this experiment. Consider any gage axis (e.g., gage axis 3) and suppose that when mounted on a structure the strains in the 3 direction have considerable variation over the gage length.

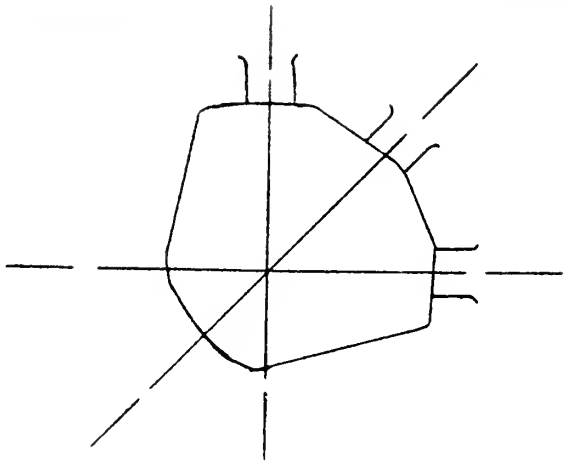

Fig. 13

The strain gage reading in the 3 direction would indicate, approximately, an average strain over the gage length, and as previously stated, it is assumed that the resulting strain is representative of the strain at the gage axes intersection However, it is quite possible that a truer location of the resulting strain would be somewhat to the right of the gage axes intersection point, especially if the lead in wires to the gage have a portion glued to the surface of the structure. From close observance of Figure 13, it appears that the true location of the resulting strain may be as much as a quarter of an inch to the right of the gage axis intersection point. In usual applications of strain gages this error would be negligible, however, as previously mention, in the subject test the strains might vary considerably over the distance of onle one-quarter inch. This error, if present, cannot be compensated for, since if the true strain locations along the axes are not at the intersection of the axes, then data taken from the gage readings would be used for constructing one strain circle to represent three different points on the structure, which is meaningless. But such error can be discounted as the main source of error in this experiment, since such an error would not cause the abrupt changes in slope of the strain vs. load curves, in fact, the error would be linear with load. Also, there is present the fact that such error could not account for the discrepancies in the torsion test, since here the shear flows are

constant over any integral section of a cell (by integral section is meant the skin as opposed to the webs).

The error due to the local effect of the rivets could certainly be prominent for some of the gages but would not explain the discrepancies shown by gage B which was located at the middle of the center cell skin and at maximum distance from a rivet line.

The instability of the structure, wherein slippage at the riveted joints causes portions of the structure to load and unload in some unpredictable fashion remains as the possibility of the cause for the large variations in stress-load slope. A further study of Figure 12 makes this appear as a reasonable conclusion. For example, note the strains at the loads of 425, 363, and 250 pounds. Ideally, these strain values would form a straight line for each gage axis, but if a straight line is drawn between the 250 and 425 pounds strain values the 363 pounds strain value does not lay upon this straight line for any of the gage axes. The 363 pounds strain values do though, show a uniform trend upon considering that gages G, B, and C have the same gage axis direction orientation on the wing, and the 363 pounds strain values all lay to the left of the aforementioned straight line for gage axes B_1, C_1, G_1 and B_2, C_2, G_2, and to the right for gage axes B_3, C_3, and G_3. Here again is evidence that the error is not caused by either random error or error in say any one set of gage readings, but rather that the structure was behaving as the data indicates, such behavior being induced by slippage of the riveted joints.

The slippage of the riveted joints could be expected to not be continuous with load, but intermittent, such that portions of the structure would "lock" over certain load ranges, slip and lock again. Thus, it is probable that over some loading range, during

which the structure remained in a locked condition, there would be the expected stress-load linearity, and such is the case for the load range of 128 to 250 pounds. Hence, it appeared that for some load range the test data might be representative of the structure without slippage of joints. To determine this range the plot of Figure 14 was constructed. The analytical values of strain as shown there are included in Table IV. From Figure 14, it appeared that the most probable load range in which the experimental strains would representative of the actual wing without slippage was between 166 and 250 pounds. Even in this range the experimental and analytical stress-load slopes are not in agreement but this can be explained from the fact that even though the test was intended for pure bending there was some torsion entering, as indicated by the strains from gages G and F. The next step was to determine if the amount of torsion entering would compensate for the difference between experimental and analytical stress-load slopes. This was done from analysis of Figure 15.

From Figure 15 note the experimental load-strain line for gage C. This was corrected for torsion by subtracting those strains due to torsion as indicated by the shearing strains from gage G. The resulting load-strain line showed close agreement with the analytically derived line. However, the same corrections when applied to the strains of gages B and D do not give agreement between the experimental and analytical results, hence, the indication that slippage occurred over this load range also.

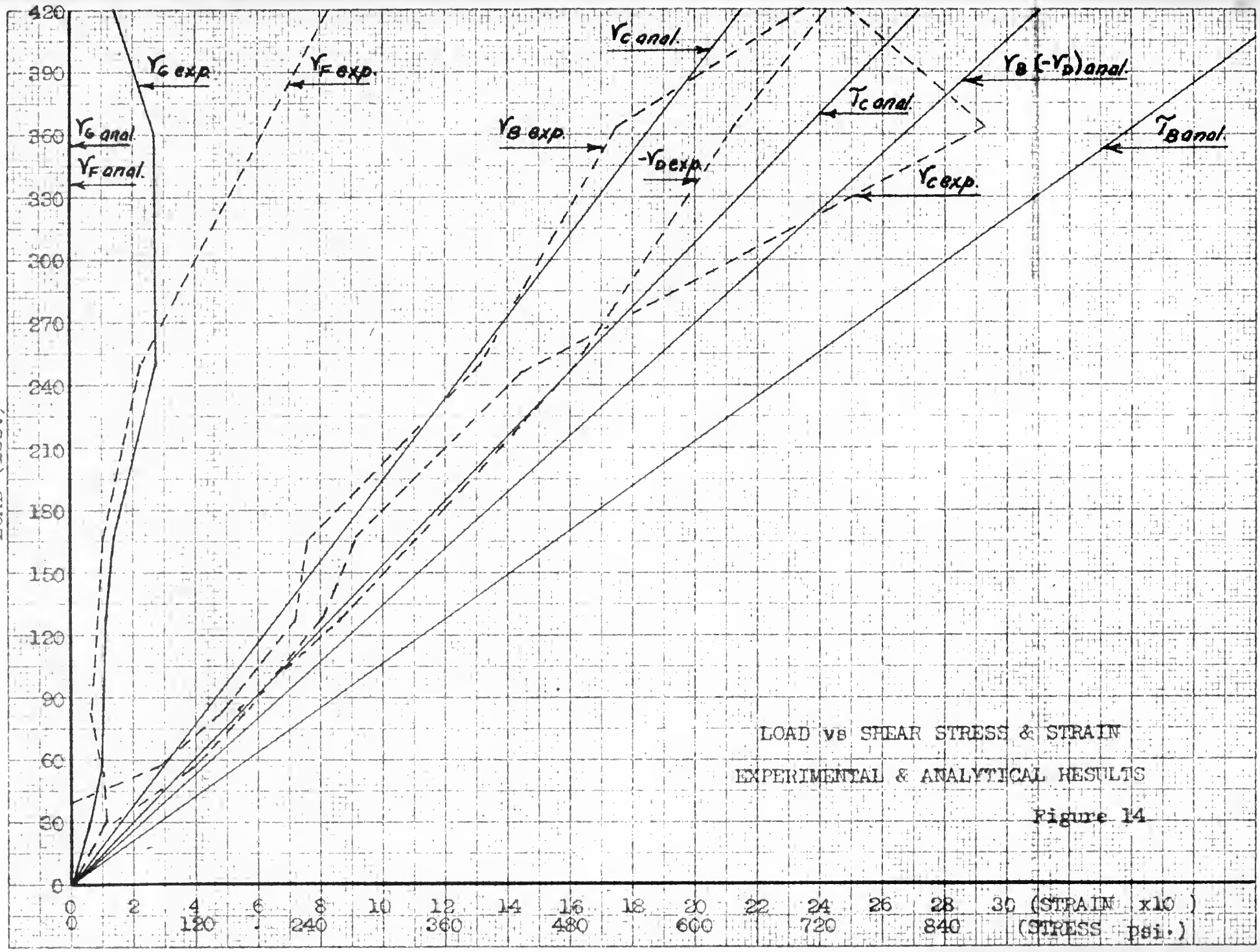

LOAD vs SHEAR STRESS & STRAIN

EXPERIMENTAL & ANALYTICAL RESULTS

Figure 14

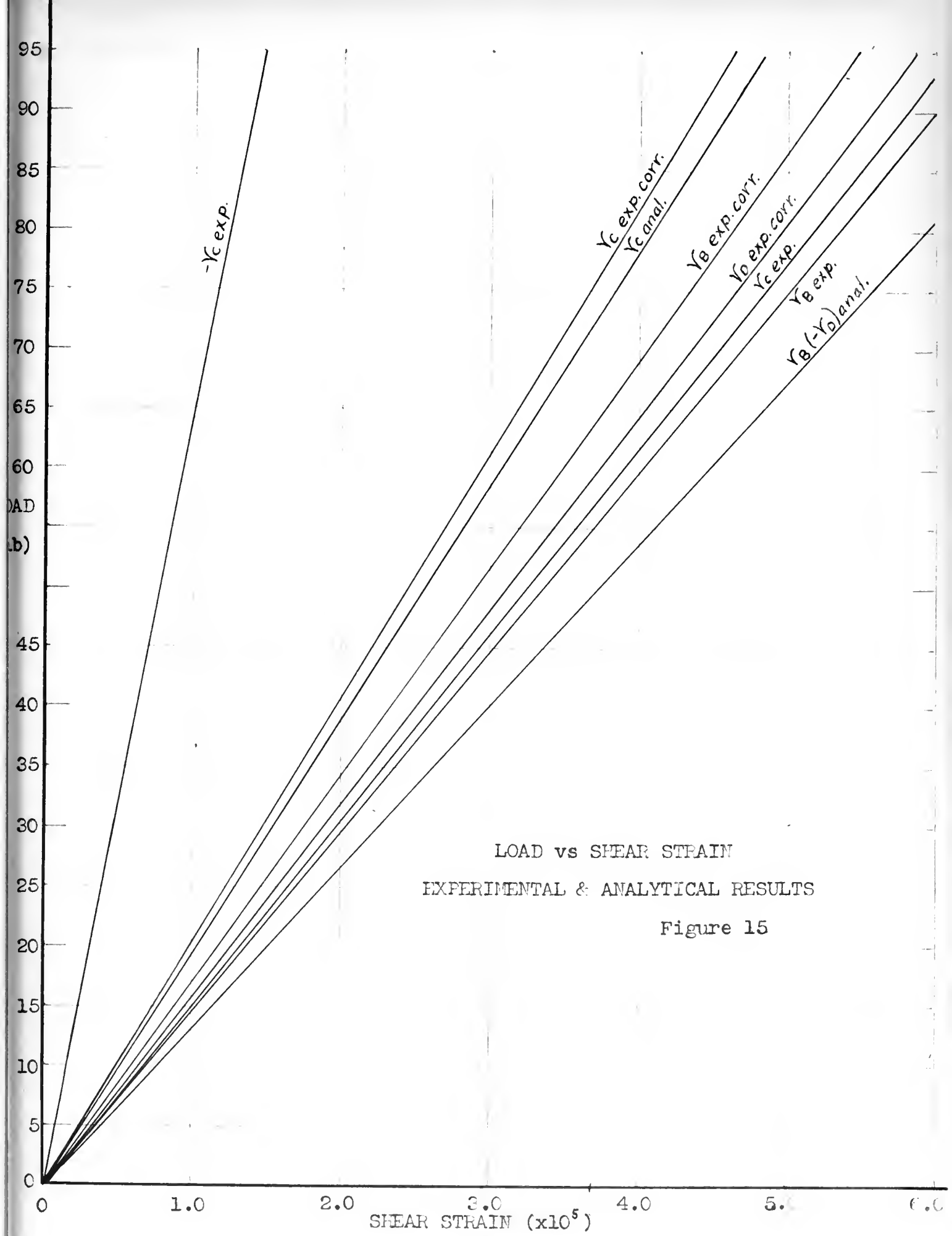

LOAD vs SHEAR STRAIN

EXPERIMENTAL & ANALYTICAL RESULTS

Figure 15

CONCLUSIONS AND RECOMMENDATIONS

The results of the static test of the wing are of little value but do indicate some recommendations for such a test. For such a test the scale of the model should be larger in order that the "life size" rivets do not predominate upon the stress distribution of the model, and also to reduce the preciseness requirement of the strain locations, as previously discussed. Also care should be taken to provide rigid joints, so that the slippage effects as evidenced by this experiment would be minimized. In fact, it appears that a different method of joining the skins at the leading and trailing edges would be preferred to riveting.

Another recommendation is to have the spar flanges as small as minimum rivet edge distance would permit. This conclusion arises a condition whereby the load transfer between spar and wing skin does not necessarily take place at the rivet line. For example, suppose that the skin-spar force relation is such that the two surfaces are being pressed upon each other, as opposed to being drawn apart. The load transfer between the two members would then be somewhat removed from the rivet line and distributed near the web end of the flange, hence, the desirability of keeping the flange width small.

The above recommendations are in no way intended as recommendations for wing construction as such, but are suggestions whereby closer agreement between analytical and experimental results might be realized.

BENDING TEST

P = Dynamometer Strain Readings. B, C, E, F, and G = Strain Gage Readings.

Strain Gage Side in Tension

P	B			C			D		
	1	2	3	1	2	3	1	2	3
362.8	689.7	485.0	472.7	439.9	417.7	394.8	734.9	429.0	242.0
364.2	619.6	484.8	472.1	444.1	419.5	392.8	734.4	430.4	243.8
365.6	695.2	488.3	471.0	453.5	423.7	389.2	733.3	433.0	247.6
366.9	697.9	490.2	470.0	460.1	426.8	387.3	731.6	434.5	249.9
369.1	704.9	495.9	472.4	468.4	431.0	384.9	730.3	436.6	253.2
371.0	707.3	496.6	470.7	475.5	434.9	384.5	729.6	438.8	255.8
375.2	711.2	499.0	466.1	491.1	442.1	377.9	726.7	443.2	262.4
380.0	720 5	505.7	465.8	507.0	449.3	371.6	724.9	448.3	269.3
384.0	727.5	510.3	463.6	521.7	456.8	366.7	722.3	452.4	276.2

Strain Gage Side in Compression

366.4	691.8	487.8	479.8	430.3	413.3	397.6	737.7	428.0	239.0
371.0	678.8	477.4	476.9	412.1	404.2	402.2	739.6	422.1	230.8
376.0	671.5	472.3	480.2	391 3	395.1	408.5	742.6	417.2	223.5
386.0	656.9	461.9	484.3	351.5	377.4	419.6	747.7	406.7	208.9

Strain Gage Side in Tension

P	E			F			G		
	1	2	3	1	2	3	1	2	3
362.8	684.4	508.8	463.0	619.3	362.5	337.3	658.3	476.8	452.2
364.2	689.0	510.3	461.9	625.2	364.2	335.9	667.7	479.5	448.8
365.6	698.0	514.0	459.0	636.6	367.8	331.6	686.2	485.2	442.1
366.9	704.5	516.6	457.1	644.6	370.5	328.6	699.2	487.9	436.7
369.1	712.6	520.2	455.0	658.3	373.7	324.9	715.7	493.6	429.5
371.0	718.8	522.9	454.1	665.0	377.3	322.2	728.3	497.4	424.8
375.2	735.0	529.8	450.5	683.3	381.5	313.5	760.3	504.2	407.7
380.0	751.8	537.2	447.4	705.1	385.7	304.1	791.3	510.2	388.9
384.0	767.2	544.3	445.3	723.8	389.5	295.2	820.6	515.5	368.6

Strain Gage Side in Compression

366.4	675.3	505.3	466.5	612.1	359.2	341.9	638.4	469.7	458.2
371.0	656.7	497.6	471 5	584.9	349.9	347.4	600.9	454.0	464.6
376.0	636.9	490.8	479.9	560.2	339.7	354.6	558.6	434.0	467.4
386.0	600.0	477.0	494.1	516.6	321.2	360.2	490.3	394.8	459.0

Strain Readings in Microinches

Table I

Table II

BENDING TEST

STRAIN GAGES (all strain readings 10^{-5})

Dyn.	lbs.		B					
			1	1	2	2	3	3
362.2	0							
362.8	12.0	0	698.7	0	485.0	0	472.7	0
364.2	41.0	29.0	691.6	1.9	484.8	-.2	472.1	- .6
365.6	69.0	57.0	695.2	5.5	488.3	3.3	471.0	-1.7
366.9	95.0	83.0	697.9	8.2	490.2	5.2	470.0	-2.7
369.1	140.0	128.0	704.9	15.2	495.9	10.9	472.1	- .6
371.0	178.0	166.0	707.3	17.6	496.6	11.6	470.7	-2.0
375.2	262.0	250.0	711.2	21.5	499.0	14.0	466.1	-6.6
380.8	375.0	363.0	720.5	30.8	505.7	20.7	465.8	-6.9
384.0	437.0	425.0	727.5	37.8	510.3	25.3	463.6	-9.1

Dyn.	lbs.		C					
			1	1	2	2	3	3
362.2	0							
362.8	12.0	0	439.9	0	417.7	0	394.8	0
364.2	41.0	29.0	444.1	4.2	419.5	1.8	392.8	-2.0
365.6	69.0	57.0	453.5	13.6	423.7	6.0	389.2	-5.6
366.9	95.0	83.0	460.1	20.2	426.8	9.1	387.3	-7.5
369.1	140.0	128.0	468.4	28.5	431.0	13.3	384.9	-9.9
371.0	178.0	166.0	475.5	35.6	434.9	17.2	384.5	-10.3
375.2	262.0	250.0	491.1	51.2	442.1	24.4	377.9	-16.9
380.8	375.0	363.0	507.0	67.1	449.3	31.6	371.6	-23.2
384.0	437.0	425.0	521.7	81.8	456.8	39.1	366.7	-28.1

Dyn.	lbs.		D					
			1	1	2	2	3	3
362.2	0							
362.8	12.0	0	734.9	0	429.9	0	242.0	0
364.2	41.0	29.0	734.4	-.5	430.4	1.4	243.8	1.8
365.6	69.0	57.0	733.3	-1.6	433.0	4.0	247.6	5.6
366.9	95.0	83.0	731.6	-3.3	434.5	5.5	249.9	7.9
369.1	140.0	128.0	730.3	-4.6	436.6	7.6	253.2	11.2
371.0	178.0	166.0	729.6	-5.3	438.8	9.8	255.8	13.8
375.2	262.0	250.0	726.7	-8.2	443.2	14.2	262.4	20.4
380.8	375.0	363.0	724.9	-10.0	448.3	19.3	269.3	27.3
384.0	437.0	425.0	722.3	-12.6	452.4	23.4	276.2	34.2

Table II BENDING TEST (Cont.)

Dyn.	lbs.		F					
			1	1	2	2	3	3
362.2	0							
362.8	12.0	0	619.3	0	362.5	0	337.3	0
364.2	41.0	29.0	625.2	5.9	364.2	1.7	335.9	-1.4
365.6	69.0	57.0	636.6	17.3	367.8	5.3	331.6	-5.7
366.9	95.0	83.0	644.6	25.3	370.5	8.0	328.6	-8.7
369.1	140.0	128.0	658.3	39.0	373.7	11.2	324.9	-12.4
371.0	178.0	166.0	665.0	45.7	377.3	14.8	322.2	-15.1
375.2	262.0	250.0	683.3	64.0	381.5	19.0	313.5	-23.8
380.8	375.0	363.0	705.1	85.8	385.7	23.2	304.1	-33.2
384.0	437.0	425.0	723.8	104.5	389.5	27.0	295.2	-42.1

Dyn.	lbs.		G					
			1	1	2	2	3	3
362.2	0							
362.8	12.0	0	658.3	0	476.8	0	452.2	0
364.2	41.0	29.0	667.7	9.4	479.5	2.7	448.8	-3.4
365.6	69.0	57.0	686.2	27.9	485.2	8.4	442.1	-10.1
366.9	95.0	83.0	699.2	40 9	487.9	11.1	436.7	-15.5
369.1	140.0	128.0	715.7	57.4	493.6	16.8	429.5	-22.7
371.0	178.0	166.0	728.3	70.0	497.4	20.6	424.8	-27.4
375.2	262.0	250.0	760.3	102.0	504.2	27.4	407.8	-44.5
380.8	375.0	363.0	791.3	133.0	510.3	33.5	388.9	-63.3
384.0	437.0	425.0	820.6	162.3	515.5	38.7	368.6	-83.6

TORSION TEST

P = Dynamometer Strain Readings

B, C, D, D, F, and G = Strain Gage Readings

P	B			C			D		
	1	2	3	1	2	3	1	2	3
354.5	691.3	494.7	480.7	435.6	416.8	399.8	732.9	423.7	237.7
355.9	690.1	493.7	480.0	435.0	416.7	399.2	733.2	423.7	237.7
357.3	690.2	499.5	480.0	435.4	427.6	397.5	733.8	417.7	236.8
361.7	690.2	512.1	479.5	436.9	451.2	391.3	735.3	405.0	235.3
365.6	690.4	524.3	479.0	437.9	474.1	387.6	736.8	391.8	234.7
368.3	692.3	532.1	479.3	438.8	487.3	384.1	737.7	385.0	234.2

P	E			F			G		
	1	2	3	1	2	3	1	2	3
354.5	680.7	508.1	465.6	615.5	358.9	337.7	648.9	470.9	450.6
355.9	680.5	508.7	466.1	613.9	358.8	337.9	648.9	470.3	450.4
357.3	680.9	514.4	464.7	614.3	371.3	337.5	647.7	482.3	450.8
361.7	681.7	529.0	463.5	614.5	396.5	333.8	646.7	516.3	449.9
365.6	682.8	544.8	463.6	613.9	417.2	327.4	645.8	528.1	446.6
368.3	683.9	554.1	464.4	614.7	427.8	321.6	645.7	539.9	443.5

Strain Readings in Microinches — Table III

CALCULATION OF EXPERIMENTAL SHEARING STRAINS

The desired shearing strains can be obtained from the following relations: $\frac{1}{2} r = \varepsilon_2 - \frac{\varepsilon_1 + \varepsilon_3}{2}$ where ε_1, ε_2, ε_3 = strain readings

or $r = 2\varepsilon_2 - (\varepsilon_1 + \varepsilon_3)$ r = shearing strain

Table IV

Shearing Strains for Bending Test
V = Applied load in pounds.

Gage C

V	$2\varepsilon_2 10^5$	$-(\varepsilon_1+\varepsilon_3) 10^5$	$r_{exp} 10^5$	$r_{anal} 10^5$
0	0	0	0	0
29	3.6	2.2	1.4	1.41
57	12.0	8.0	4.0	2.90
83	18.2	12.7	5.5	4.20
128	26.6	18.6	8.0	6.60
166	34.4	25.3	9.1	8.50
250	48.8	34.3	14.5	12.81
363	73.2	43.9	29.3	18.55
425	78.2	53.7	24.5	21.75

Gage B

V	$2\varepsilon_2 10^5$	$-(\varepsilon_1+\varepsilon_3) 10^5$	$r_{exp} 10^5$	$r_{anal} 10^5$
0	0	0	0	0
29	-.4	1.3	-1.7	2.10
57	6.6	3.8	2.8	4.20
83	10.4	5.5	4.9	6.22
128	21.8	14.6	7.2	9.55
166	23.2	15.6	7.6	12.25
250	28.0	14.9	13.1	18.50
363	41.4	23.9	17.5	26.90
425	50.6	28.7	21.9	31.50

Gage D

V	$2\varepsilon_2 10^5$	$-(\varepsilon_1+\varepsilon_3) 10^5$	$r_{exp} 10^5$	$r_{anal} 10^5$
0	0	0	0	0
29	2.8	1.3	1.5	2.10
57	8.0	4.0	4.0	4.20
83	11.0	4.6	5.4	6.22
128	15.2	6.6	8.6	9.55
166	19.6	8.5	11.1	12.25
250	28.4	12.2	16.2	18.5
363	38.6	17.3	21.3	26.9
425	46.8	22.4	24.4	31.6

Gage G

0	0	0	0	0
29	5.4	6.0	-.6	0
57	16.8	17.8	-1.0	0
83	22.3	25.4	-3.2	0
128	33.6	34.7	-1.1	0
166	41.2	42.6	-1.4	0
250	54.8	57.5	-2.7	0
363	67.0	69.7	-2.7	0
425	77.4	78.7	-1.3	0

Gage F

0	0	0	0	0
29	3.4	4.5	-1.1	0
57	10.6	11.6	-1.0	0
83	16.0	16.6	-0.6	0
128	22.4	26.6	-4.2	0
166	29.6	30.6	-1.0	0
250	38.0	40.2	-2.2	0
363	46.4	52.6	-6.2	0
425	54.0	62.4	-8.4	0